PERGAMON

International Journal of Heat and Mass Transfer 46 (2003) 55–69

International Journal of HEAT and MASS TRANSFER

www.elsevier.com/locate/ijhmt

Study of heat transfer in multilayered structure within the framework of dual-phase-lag heat conduction model using lattice Boltzmann method

Jeng-Rong Ho *, Chun-Pao Kuo, Wen-Shu Jiaung

Department of Mechanical Engineering, National Chung Cheng University, Chia-Yi, Taiwan 621, China

Received 22 August 2001; received in revised form 30 June 2002

Abstract

The effect of the phase lag of temperature gradient, τ_T, on the transmission–reflection phenomenon, induced by a pulsed thermal energy passing the interface of a two-layered structure, within the framework of dual-phase-lag based heat conduction equation is studied numerically by the lattice Boltzmann (LB) method. An extended LB equation, with truncation error of order two, and a numerical solution procedure are developed for the solution of the governing equation and the derived interfacial boundary condition. Results show that the interface reflects a negative followed by a positive waveform when the pulsed thermal wave propagates from the media with lower τ_T into the media with higher τ_T and vice versa if the wave propagates from higher into lower τ_T media. These special phenomena which have not been presented in the available literatures are unable to be predicted in the framework of hyperbolic heat conduction equation.

1. Introduction

Although Fourier's law is appropriate in describing heat conduction in most common engineering situations, however, it breaks down in situations involving very short times, high heat fluxes, and at very low temperatures [1]. The anomaly of this classical theory is from the assumption that the heat flux vector and the temperature gradient across a material volume occur at the same instant of time. Such an immediate response results in an infinite speed of heat propagation. In order to associate a finite heat propagation speed, Cattaneo [2] and Vernotte [3] modified Fourier's law by including a relaxation model that, in parallel to Fourier's law, can be written as [4]

$$\mathbf{q}(\xi, \eta + \tilde{\tau}_q) = -k\nabla\theta(\xi, \eta). \tag{1}$$

This equation shows that the temperature gradient $\nabla\theta$ established at a position ξ at time η results in a heat flux to flow at the same position but at a different instant of time $\eta + \tilde{\tau}_q$. Physically, $\tilde{\tau}_q$ represents the relaxation time or the phase-lag time between the temperature gradient and the commencement of heat flow in a medium. This modified Fourier's law incorporating with the conservation of energy leads to the wave-based hyperbolic heat conduction equation (HHCE). For some initial or boundary conditions, the HHCE will introduce a sharp wavefront in the history of wave propagation, resulting in several physical phenomena which cannot be depicted by diffusion. Comprehensive literature surveys of heat waves until the eighties can be found in the review articles by Joseph and Preziosi [5,6] and more recently by Ozisik and Tzou [7].

* Corresponding author. Tel.: +886-5-272-0411x33316; fax: +886-5-272-0589.
E-mail address: imejrho@ccu.edu.tw (J.-R. Ho).

0017-9310/03/$ - see front matter
PII: S0017-9310(02)00260-0

Nomenclature

A	coefficient $(= 1/(b+1))$
B	dimensionless parameter $(= \tau_T/w\tau_q)$
b	number of propagation direction in a lattice
C_p	dimensionless specific heat at constant pressure
c_p	specific heat at constant pressure
$\mathbf{e}_i$	propagation velocity in direction i in a lattice
e	propagation speed $(= \Delta x/\Delta t)$
f_i	particle distribution function in the $\mathbf{e}_i$ direction
$f_i^{(0)}$	equilibrium particle distribution function in the $\mathbf{e}_i$ direction
G	dimensionless heat source per unit volume
g	heat source per unit volume
K	dimensionless thermal conductivity
k	thermal conductivity
L	dimensionless length of slab
l	dimensionless spatial range where the pulsed energy imposed
O	order of magnitude
$\mathbf{q}$	heat flux
q	scalar of heat flux
R	dimensionless density
R_E	truncation error
T	dimensionless temperature
t	dimensionless time
V	speed of thermal wave
x	dimensionless space variable

Greek symbols

α	thermal diffusivity
Γ	dimensionless thermal diffusivity
γ	parameter $(= \Gamma/2(\tau - \Delta t/2))$
δ	width of the volumetric heat source
$\delta(t)$	Dirac delta function
ε	small quantity for Chapman–Enskog expansion
η	time
θ	temperature
λ	parameter$(= \Gamma/(\tau - \Delta t/2))$
ξ	space variable
ρ	density
τ	relaxation time in BGK model
τ_q	dimensionless phase lag of the heat flow
τ_T	dimensionless phase lag of the temperature gradient
$\tilde{\tau}_q$	phase lag of the heat flow
$\tilde{\tau}_T$	phase lag of the temperature gradient
Ψ	source term in lattice Boltzmann equation
Δx	dimensionless lattice size
Δt	dimensionless time step

Superscripts

(1)	$O(\varepsilon)$ in the Chapman–Enskog expansion
(2)	$O(\varepsilon^2)$ in the Chapman–Enskog expansion

Subscripts

I	Layer 1
II	Layer 2

i	direction i in a lattice
j	lattice index
r	reference state for dimensionless parameter

Although the HHCE can solve the paradox of instantaneous response of thermal disturbance, it also introduces some unusual behaviors [8] and physically impossible solutions [9,10]. Instead of the precedence assumption in Eq. (1), assuming the lead of the temperature gradient to the heat flux, a more general model, the dual-phase-lag (DPL) model, was proposed by Tzou [4,11,12]. This model allows either the temperature gradient to precede the heat flux or the heat flux to precede the temperature gradient. Mathematically, the constitutive law for DPL is represented by

$$\mathbf{q}(\xi,\eta+\tilde{\tau}_q) = -k\nabla\theta(\xi,\eta+\tilde{\tau}_T), \tag{2}$$

where $\tilde{\tau}_T$ is the phase lag of the temperature gradient. Ever since its agreement with experimental results was shown [13], the DPL model has attracted a considerable interest in the fundamental transport process of heat and mass including, for example, thermal stresses of thin plate [14], lagging behavior of heat transport in amorphous materials [15], semi-infinite slab with surface heat flux [16], nonequilibrium entropy production [17,18], thermalization and relaxation during short-time transient in microscale [19,20], temperature-dependent thermal lagging under ultrafast laser heating [21], and, more recently, the growth of interfacial phase compound in metal matrix composites as well as in thin films [22–24].

In this exposition, we shall study the propagation of an ultrashort pulsed energy across the solid-solid interface of dissimilar material layers. With the advent of modern laser with ultrashort pulse duration, picosecond or femtosecond, the ultrafast heat transport process has become an important problem with practical importance [25]. Many interesting phenomena and unusual results regarding energy transport at interface of dissimilar materials have been explored [7,26–29]. Most of them, however, were within the framework of HHCE, that is, attentions were mainly on the effect of $\tilde{\tau}_q$. No researches, to authors' best knowledge, had focused on the effect of $\tilde{\tau}_T$ on the energy disposition at layer interface. Mathematically, the DPL model introduces additional high-order, mixed spatial and time derivative terms in the governing equation as well as in boundary condition at the layer interface. In additional to the mathematical difficulties, the propagation of pulsed energy for multilayered regions may provide additional insight and understanding into the special phenomena of heat propagation in the framework of the DPL model.

In the present study, both the heat transfer and the transmission–reflection phenomenon at interface induced by an instantaneous energy pulse incident on the surface of a two-layered structure are studied. The dimensionless governing equation and the interfacial condition based on the continuities of temperature and heat flux in the framework of DPL model are first derived and discussed. Subsequently, an extended, discretized lattice Boltzmann (LB) method, represented by the BGK (Bhatnagar–Gross–Krook) approximation [37] with a source term, is proposed for the governing equation. The technique of Chapman–Enskog multiscale expansion is employed to demonstrate that the proposed extended LB equation macroscopically matches the governing equation with truncation error of order two. A numerical solution procedure to link the governing equation and the initial, interfacial as well as boundary conditions is developed. Part of the transmission–reflection-combination phenomenon based on the HHCE presented in the literature [1] is retrieved to verify the validity of the present numerical scheme. Finally, effects of $\tilde{\tau}_T$ on the transmission–reflection phenomena at layer interface are presented. The special phenomena obtained within the DPL-based heat conduction equation are discussed.

2. Physical model and mathematical formulation

Shown in Fig. 1, a one-dimensional, two-layered structure without contact resistance is considered. It is further assumed that these two layers are of the same thickness but with different material properties. At time $\eta = 0$, an energy pulse incidents on the surface of the two-layered structure and is absorbed within a penetration depth δ in Layer I. This system is highly promising in laser processing of thin-film materials [30–32]. Instantaneously after the energy pulsed, $\eta = 0^+$, the absorbed energy within δ is released and propagates into the mulitlayered structure, the positive ξ direction.

Eq. (2) couples with equation of energy conservation leading to the heat conduction equation based on the DPL model as

$$\tilde{\tau}_q\frac{\partial^2\theta}{\partial\eta^2}+\frac{\partial\theta}{\partial\eta} = \alpha\frac{\partial^2\theta}{\partial\xi^2}+\alpha\tilde{\tau}_T\frac{\partial^3 T}{\partial\xi^2\partial\eta}+\frac{\tilde{\tau}_q}{\rho c_p}\frac{\partial g}{\partial\eta}+\frac{g}{\rho c_p}. \tag{3}$$

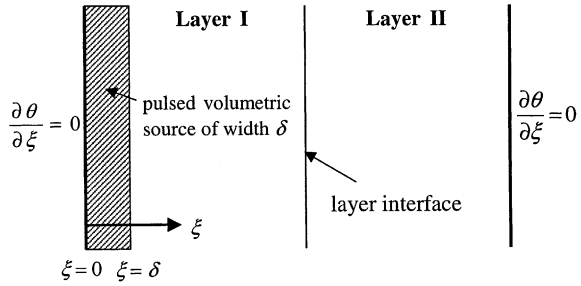

Fig. 1. Schematic diagram of the physical system showing the two-layered structure, coordinate, boundary condition and the depth of the pulsed volumetric heat source.

Eq. (3) reduces to the HHCE if $\tilde{\tau}_T = 0$, and it becomes the classical heat diffusion equation when $\tilde{\tau}_T = \tilde{\tau}_q = 0$. With introducing the following dimensionless variables

$$\begin{aligned} &R = \rho/\rho_{\mathrm{r}}, \quad C_p = c_p/c_{pr}, \quad K = k/k_{\mathrm{r}}, \quad \Gamma = \alpha/\alpha_{\mathrm{r}}, \quad \tau_q = \tilde{\tau}_q/\tilde{\tau}_{q_{\mathrm{r}}}, \quad \tau_T = \tilde{\tau}_T/\tilde{\tau}_{q_{\mathrm{r}}}, \\ &V = \sqrt{\Gamma/\tau_q}, \quad t = \eta/2\tilde{\tau}_{q_{\mathrm{r}}}, \quad x = \xi/2\sqrt{\alpha_{\mathrm{r}}\tilde{\tau}_{q_{\mathrm{r}}}}, \quad T = \theta/\theta_{\mathrm{r}}, \quad G = \frac{4\tilde{\tau}_{q_{\mathrm{r}}} g}{\rho c_p \theta_{\mathrm{r}}}, \end{aligned} \tag{4}$$

the dimensionless form of Eq. (3) is given by

$$\frac{\partial^2 T}{\partial t^2} + \frac{2}{\tau_q}\frac{\partial T}{\partial t} = V^2\frac{\partial^2 T}{\partial x^2} + \Gamma B\frac{\partial^3 T}{\partial x^2 \partial t} + \frac{1}{2}\frac{\partial G}{\partial t} + \frac{G}{\tau_q}, \tag{5}$$

where B is a dimensionless parameter that characterizes the lagging response and is defined as the ratio between the two phase lags, $B = \tau_T/2\tau_q$.

In this study, it is assumed that both initial temperature and initial rate of temperature change in the entire computational domain are uniform, that is,

$$T(x,0) = 0, \frac{\partial T(x,0)}{\partial t} = 0 \quad \text{for all } x. \tag{6}$$

We consider the situation that two sides of the structure are insulated. The expression for adiabatic boundary condition within the framework of DPL model can be derived through the constitutive equation, Eq. (2). The general solution of heat flux was given by [17]

$$\mathbf{q}(x,t) = \mathbf{q}(x,0)\mathrm{e}^{-t/\tau_q} + k\frac{\tau_T}{\tau_q}\mathrm{e}^{-t/\tau_q}\nabla T(x,0) - k\frac{\tau_T}{\tau_q}\nabla T(x,t) - \frac{k}{\tau_q}\left(1 - \frac{\tau_T}{\tau_q}\right)\int_0^{\mathrm{t}} \mathrm{e}^{-(t-\upsilon)/\tau_q}\nabla T(x,\upsilon)\,\mathrm{d}\upsilon. \tag{7}$$

Physically, the adiabatic conditions means no heat flux is able to pass through the boundaries, that is, $\mathbf{q} = 0$ at both $x = 0$ and L for all t. Initially, neither temperature gradient nor heat flux is in the slab, ∇T and $\mathbf{q}$ are equal to zero at $t = 0$. Thus, the first two terms on the right hand side of Eq. (7) are vanishing. To satisfy $\mathbf{q} = 0$ for all t at two boundaries, we have $\nabla T = 0$, i.e.,

$$\frac{\partial T(0,t)}{\partial x} = \frac{\partial T(L,t)}{\partial x} = 0. \tag{8}$$

At the interface of the two layers, $x = L/2$, two continuous conditions to implement are the continuities of temperature and heat flux. They are expressed as

$$T_{\mathrm{I}} = T_{\mathrm{II}} \quad \text{and} \quad \mathbf{q}_{\mathrm{I}} = \mathbf{q}_{\mathrm{II}} \qquad \text{at } x = L/2 \quad \text{for all } t. \tag{9}$$

These interfacial conditions simply imply there is neither thermal resistance nor thermal inertia at the interface. Using Taylor's series expansion to the first order of Eq. (2), the interfacial condition $\mathbf{q}_{\mathrm{I}} = \mathbf{q}_{\mathrm{II}}$ can be expressed in terms of temperature as

$$-K_{\mathrm{I}}\left[\left(\tau_{q_{\mathrm{II}}}\frac{\partial^2 T_{\mathrm{I}}}{\partial x \partial t} + \frac{\partial T_{\mathrm{I}}}{\partial x}\right) + \tau_{T_{\mathrm{I}}}\frac{\partial}{\partial t}\left(\tau_{q_{\mathrm{II}}}\frac{\partial^2 T_{\mathrm{I}}}{\partial x \partial t} + \frac{\partial T_{\mathrm{I}}}{\partial x}\right)\right] = -K_{\mathrm{II}}\left[\left(\tau_{q_{\mathrm{I}}}\frac{\partial^2 T_{\mathrm{II}}}{\partial x \partial t} + \frac{\partial T_{\mathrm{II}}}{\partial x}\right) + \tau_{T_{\mathrm{II}}}\frac{\partial}{\partial t}\left(\tau_{q_{\mathrm{I}}}\frac{\partial^2 T_{\mathrm{II}}}{\partial x \partial t} + \frac{\partial T_{\mathrm{II}}}{\partial x}\right)\right]. \tag{10}$$

As the DPL model covers both hyperbolic and parabolic heat conduction equations, Eq. (10) represents the general form of continuity of heat flux at the interface of two adjacent regions with ideal thermal contact. When $\tau_{T_\mathrm{I}} = \tau_{T_\mathrm{II}}$, Eq. (10) reduces to

$$K_\mathrm{I}\left(\tau_{q_\mathrm{II}}\frac{\partial^2 T_\mathrm{I}}{\partial x\,\partial t}+\frac{\partial T_\mathrm{I}}{\partial x}\right)=K_\mathrm{II}\left(\tau_{q_\mathrm{I}}\frac{\partial^2 T_\mathrm{II}}{\partial x\,\partial t}+\frac{\partial T_\mathrm{II}}{\partial x}\right). \tag{11}$$

This is the interfacial condition for HHCE [1]. Eq. (11) can further reduce to the interfacial condition for parabolic heat conduction equation, $K_\mathrm{I}\partial T_\mathrm{I}/\partial x = K_\mathrm{II}\partial T_\mathrm{II}/\partial x$, when $\tau_{q_\mathrm{I}} = \tau_{q_\mathrm{II}}$.

3. Numerical method

To solve the propagation of pulsed energy in a two-layered structure in the framework of the DPL model, the field equation, Eq. (5), should be solved together with initial, boundary and interfacial equations described respectively by Eqs. (6), (8) and (10). The LB method is adopted in this study for its ability to handle complex boundary condition and capability to avoid numerical instability. Recently this method has been considered as a powerful tool for the solution of partial differential equation and simulation of complicated physical problems [33–40]. The use of LB method for the parabolic heat conduction equation was first proposed by Wolf-Gladrow [39] and we presented the LB method for Stefan problem in the framework of parabolic heat conduction equation [40].

3.1. The extended lattice Boltzmann equation

The starting point of the LB method is the kinetic equation for the particle distribution function, $f_i(x,t)$,

$$f_i(\mathbf{x}+\mathbf{e}_i\Delta t, t+\Delta t)-f_i(\mathbf{x},t)=-\frac{\Delta t}{\tau}\left[f_i(\mathbf{x},t)-f_i^{(0)}(\mathbf{x},t)\right],\quad i=0,1,\ldots b, \tag{12}$$

where f_i is the particle distribution functions denote the number of particles at lattice node $\mathbf{x}$ and time t, moving in direction i with velocity $\mathbf{e}_i$ along the lattice link $\Delta\mathbf{x}_i = \mathbf{e}_i\Delta t$ connecting nearest neighbors. The first term on the right hand side represents collisions from b directions that drive each distribution f_i toward its local equilibrium distribution $f_i^{(0)}$ in a dimensionless time lapse of $\Delta t/\tau$. Once the discrete populations are known, the macroscopic physical quantity $\tau_q\partial T(\mathbf{x},t)/\partial t$ can be expressed in terms of the discrete distribution function f_i as

$$\tau_q\frac{\partial T(\mathbf{x},t)}{\partial t}=\sum_i f_i(\mathbf{x},t). \tag{13}$$

As the first order temperature derivative with respect to time has been obtained, the local temperature at time $t+\Delta t$ can be obtained through the Taylor expansion up to the second order as

$$T(\mathbf{x},t+\Delta t)=T(\mathbf{x},t)+\Delta t\frac{\partial T(\mathbf{x},t)}{\partial t}+\frac{\Delta t^2}{2}\frac{\partial^2 T(\mathbf{x},t)}{\partial t^2}+\mathrm{O}(\Delta t^3). \tag{14}$$

By analogy with the source term in Eq. (5), some source term are introduced to the LB equation and the resulting extended LB equation is proposed as

$$f_i(\mathbf{x}+\mathbf{e}_i\Delta t, t+\Delta t)-f_i(\mathbf{x},t)=-\frac{\Delta t}{\tau}\left[f_i(\mathbf{x},t)-f_i^{(0)}(\mathbf{x},t)\right]-2A\Delta t\frac{\partial T}{\partial t}+\Delta t\Psi. \tag{15}$$

In Eq. (17), $f_i^{(0)}$ is the equilibrium, directional particle distribution function, A is a coefficient to be determined, Ψ is determined from external heat source.

3.2. Chapman–Enskog expansion

The macroscopic consistence between Eqs. (5) and (15) can be demonstrated through the Chapman–Enskog expansion [37,38]. In this expansion the particle distribution functions, f_i, are expanded up to the third order with respect to the expansion parameter ε as

$$f_i = f_i^{(0)}+\varepsilon f_i^{(1)}+\varepsilon^2 f_i^{(2)}+\varepsilon^3 f_i^{(3)}+\mathrm{O}(\varepsilon^4), \tag{16}$$

where ε is a small quantity, i.e. $|\varepsilon| \ll 1$. The summation of distribution functions satisfy

$$\sum_i f_i = \sum_i f_i^{(0)} \quad \text{and} \quad \sum_i f_i^{(1)} = \sum_i f_i^{(2)} = \sum_i f_i^{(3)} = 0. \tag{17}$$

Time and space scales involved in the changes of quantities are the large spatial scale $x^{(1)}$ the fast time scale $t^{(1)}$ and the slow time scale $t^{(2)}$ [37,41]. These suggest the following scaling

$$\partial_t \approx \varepsilon \partial_{t^{(1)}} + \varepsilon^2 \partial_{t^{(2)}} + \varepsilon^3 \partial_{t^{(3)}} + \mathrm{O}(\varepsilon^4), \tag{18}$$

$$\partial_x \approx \varepsilon \partial_{x^{(1)}} + \mathrm{O}(\varepsilon^2). \tag{19}$$

The heat dissipation and source terms in Eq. (15) are assumed in the scale of $\mathrm{O}(\varepsilon^2)$ which can be accomplished through

$$\begin{aligned} &\frac{\partial T}{\partial t} \approx \varepsilon^2 \frac{\partial T}{\partial t^{(2)}} \\ &\Psi = \varepsilon^2 \psi. \end{aligned} \tag{20}$$

Expanding $f_i(\mathbf{x} + \mathbf{e}_i \Delta t, t + \Delta t)$ in Eq. (15) around $f_i^{(0)}(\mathbf{x}, t)$ up to $\mathrm{O}(\Delta t^3)$ and introducing the above suggested scales, the resulting equations to order of ε, ε^2 and ε^3 are given as:

$$\partial_{t^{(1)}} f_i^{(0)} + \partial_{x_\alpha^{(1)}} e_{i\alpha} f_i^{(0)} = -\frac{1}{\tau} f_i^{(1)}, \tag{21}$$

$$\partial_{t^{(2)}} f_i^{(0)} + \left(-\tau + \frac{\Delta t}{2} \right) \left(\partial_{t^{(1)}} + \partial_{x_\alpha^{(1)}} e_{i\alpha} \right)^2 f_i^{(0)} = -\frac{1}{\tau} f_i^{(2)} - 2A \frac{\partial T}{\partial t^{(2)}} + \psi, \tag{22}$$

and,

$$\begin{aligned} &\partial_{t^{(3)}} f_i^{(0)} + (-2\tau + \Delta t) \left(\partial_{t^{(1)}} + \partial_{x_\alpha^{(1)}} e_{i\alpha} \right) \partial_{t^{(2)}} f_i^{(0)} + \left(\tau^2 - \tau \Delta t + \frac{\Delta t^2}{6} \right) \left(\partial_{t^{(1)}} + \partial_{x_\alpha^{(1)}} e_{i\alpha} \right)^3 f_i^{(0)} \\ &\quad = -\frac{1}{\tau} f_i^{(3)} + 2\tau A \left(\partial_{t^{(1)}} + \partial_{x_\alpha^{(1)}} e_{i\alpha} \right) \frac{\partial T}{\partial t^{(2)}} - \tau \left(\partial_{t^{(1)}} + \partial_{x_\alpha^{(1)}} e_{i\alpha} \right) \psi, \end{aligned} \tag{23}$$

respectively. Summing Eqs. (21)–(23) over i from 0 to b leads to

$$\tau_q \partial_{t^{(1)}} \frac{\partial T}{\partial t} + \partial_{x_\alpha^{(1)}} \sum_{i=0}^{b} e_{i\alpha} f_i^{(0)} = 0, \tag{24}$$

$$\begin{aligned} &\tau_q \partial_{t^{(2)}} \frac{\partial T}{\partial t} + \left(\frac{\Delta t}{2} - \tau \right) \left[\tau_q \partial_{t^{(1)}} \partial_{t^{(1)}} \frac{\partial T}{\partial t} + 2 \partial_{t^{(1)}} \partial_{x_\alpha^{(1)}} \sum_{i=0}^{b} e_{i\alpha} f_i^{(0)} + \partial_{x_\alpha^{(1)}} \partial_{x_\beta^{(1)}} \sum_{i=0}^{b} e_{i\alpha} e_{i\beta} f_i^{(0)} \right] \\ &\quad = -2A(b+1) \partial_{t^{(2)}} T + (b+1) \psi, \end{aligned} \tag{25}$$

and

$$\begin{aligned} &\tau_q \partial_{t^{(3)}} \frac{\partial T}{\partial t} + (\Delta t - 2\tau) \left(\tau_q \partial_{t^{(1)}} \partial_{t^{(2)}} \frac{\partial T}{\partial t} + \partial_{x_\alpha^{(1)}} \partial_{t^{(2)}} \sum_{i=0}^{b} e_{i\alpha} f_i^{(0)} \right) + \left(\tau^2 - \tau \Delta t + \frac{\Delta t^2}{6} \right) \left(\tau_q \partial_{t^{(1)}} \partial_{t^{(1)}} \partial_{t^{(1)}} \frac{\partial T}{\partial t} \right. \\ &\quad \left. + 3 \partial_{t^{(1)}} \partial_{t^{(1)}} \partial_{x_\alpha^{(1)}} \sum_{i=0}^{b} e_{i\alpha} f_i^{(0)} + 3 \partial_{t^{(1)}} \partial_{x_\alpha^{(1)}} \partial_{x_\beta^{(1)}} \sum_{i=0}^{b} e_{i\alpha} e_{i\beta} f_i^{(0)} + \partial_{x_\alpha^{(1)}} \partial_{x_\beta^{(1)}} \partial_{x_\gamma^{(1)}} \sum_{i=0}^{b} e_{i\alpha} e_{i\beta} e_{i\gamma} f_i^{(0)} \right) \\ &\quad = 2\tau A \left[(b+1) \partial_{t^{(1)}} \partial_{t^{(2)}} T + \partial_{t^{(2)}} \partial_{x_\alpha^{(1)}} \sum_{i=0}^{b} e_{i\alpha} T \right] - \tau \left[(b+1) \partial_{t^{(1)}} \psi + \partial_{x_\alpha^{(1)}} \sum_{i=0}^{b} e_{i\alpha} \psi \right]. \end{aligned} \tag{26}$$

Taking (24) $\times \varepsilon +$ (25) $\times \varepsilon^2 +$ (26) $\times \varepsilon^3$ and using the following constraints

$$\begin{aligned} &\sum_{i=0}^{b} e_{i\alpha} f_i^{(0)} = 0 \\ &\sum_{i=0}^{b} e_{i\alpha} e_{i\beta} f_i^{(0)} = \lambda T + \tau_T \gamma \frac{\partial T}{\partial t}, \\ &\sum_{i=0}^{b} e_{i\alpha} e_{i\beta} e_{i\gamma} f_i^{(0)} = 0, \end{aligned} \tag{27}$$

we obtain

$$\tau_q \frac{\partial^2 T}{\partial t^2} + 2A(b+1)\frac{\partial T}{\partial t} = \left(\tau - \frac{\Delta t}{2}\right)\lambda \frac{\partial^2 T}{\partial x^2} + \left(\tau - \frac{\Delta t}{2}\right)\tau_T \gamma \frac{\partial^3 T}{\partial t \partial x^2} + (b+1)\Psi + 2\tau A\varepsilon^3(b+1)\partial_{t^{(1)}}\partial_{t^{(2)}} T - \tau\varepsilon^3(b+1)\partial_{t^{(1)}}\psi - 3\varepsilon^3\left(\tau^2 - \tau\Delta t + \frac{\Delta t^2}{6}\right)\partial_{t^{(1)}}\partial_{x_\alpha^{(1)}}\partial_{x_\beta^{(1)}}\left(\lambda T + \tau_T \gamma \frac{\partial T}{\partial t}\right) + \mathrm{O}(\Delta t^3) + \mathrm{O}(\varepsilon^4). \quad (28)$$

As Δt and ε are approaching to zero, Eq. (28) is consistent with Eq. (5) if A, λ, γ, and Ψ are chosen as

$$\begin{aligned} A &= \frac{1}{b+1}, \\ \lambda &= \frac{\tau_q V^2}{(\tau - \Delta t/2)} = \frac{\Gamma}{(\tau - \Delta t/2)}, \\ \gamma &= \frac{\Gamma}{2(\tau - \Delta t/2)}, \\ \Psi &= \frac{1}{b+1}\left(G + \frac{\tau_q}{2}\frac{\partial G}{\partial t}\right), \end{aligned} \quad (29)$$

with truncation error

$$R_{\mathrm{E}} = 2\tau A\varepsilon^3(b+1)\partial_{t^{(1)}}\partial_{t^{(2)}} T - \tau\varepsilon^3(b+1)\partial_{t^{(1)}}\psi - 3\varepsilon^3\left(\tau^2 - \tau\Delta t + \frac{\Delta t^2}{6}\right)\partial_{t^{(1)}}\partial_{x_\alpha^{(1)}}\partial_{x_\beta^{(1)}}\left(\lambda T + \tau_T \gamma \frac{\partial T}{\partial t}\right) + \mathrm{O}(\Delta t^3) + \mathrm{O}(\varepsilon^4). \quad (30)$$

The D1Q3 lattice, schematically shown in Fig. 2, with $b = 2$, $\mathbf{e}_0 = 0$, $\mathbf{e}_1 = e\hat{\mathbf{i}}$ and $\mathbf{e}_2 = -e\hat{\mathbf{i}}$ is used for this one-dimensional study. The equilibrium particle distribution function, $f_i^{(0)}$, are able to be obtained by $\sum_{i=0}^{b} f_i^{(0)} = \tau_q \partial T/\partial t$ and conditions given in Eq. (27) which yield

$$\begin{aligned} f_0^{(0)} &= \tau_q \frac{\partial T}{\partial t} - \frac{\lambda}{e^2} T - \frac{\tau_T \gamma}{e^2}\frac{\partial T}{\partial t}, \\ f_1^{(0)} &= f_2^{(0)} = \frac{\lambda}{be^2} T + \frac{\tau_T \gamma}{be^2}\frac{\partial T}{\partial t}. \end{aligned} \quad (31)$$

3.3. Implementation of initial, interfacial, and boundary conditions

The initial distribution function $f_i(\mathbf{x}, 0)$ are calculated using one term in the expansion expression of Eq. (16), that is, $f_i(\mathbf{x}, 0)$ was set to be $f_i^{(0)}(\mathbf{x}, 0)$ which, according to Eq. (31), depend on the initial temperature and initial rate of temperature change. The adiabatic boundary condition is implemented as the particle distribution function is reflected specularly [42]. That is, $f_1 = f_2$ at $x = 0$ and $f_2 = f_1$ at $x = L$.

For a prescribed temperature at boundary, the particle distribution function is set to be equal to the equilibrium particle distribution function corresponding to that temperature. According to Eq. (31), in addition to the temperature, T, the rate of change of temperature, $\partial T/\partial t$, is also required. The rate of temperature change is numerically implemented through a rapid transient of linear temperature rise with time [43]. The rise time is made very small, of the order of 10^{-100}, so that the boundary closely approximates a step change in temperature.

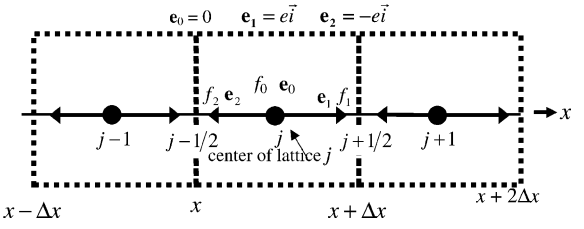

Fig. 2. Schematic diagram showing the one-dimensional D1Q3 lattice. Three velocities, $\mathbf{e}_0$, $\mathbf{e}_1$, and $\mathbf{e}_2$ are used for this lattice. f_0, f_1, and f_2 represent particle distribution functions propagating respectively in the $\mathbf{e}_0$, $\mathbf{e}_1$, and $\mathbf{e}_2$ directions.

At the interface, $x = L/2$, both temperature and heat flux are continuous. These conditions can be accomplished through letting $T_{\mathrm{I}} = T_{\mathrm{II}} = T(L/2,t)$ in Eq. (10). The rate of temperature change can be obtained by discretization Eq. (10) using first-order finite difference scheme in both space and time as

$$\begin{aligned}\frac{\partial T(L/2,t)}{\partial t} = {} & \frac{1}{\left(K_{\mathrm{I}}\tau_{q_{\mathrm{II}}} + \frac{K_{\mathrm{I}}\tau_{q_{\mathrm{II}}}\tau_{T_{\mathrm{I}}}}{\Delta t} + K_{\mathrm{I}}\tau_{T_{\mathrm{I}}} + K_{\mathrm{II}}\tau_{q_{\mathrm{I}}} + \frac{K_{\mathrm{II}}\tau_{q_{\mathrm{I}}}\tau_{T_{\mathrm{II}}}}{\Delta t} + K_{\mathrm{II}}\tau_{T_{\mathrm{II}}}\right)}\left[\left(K_{\mathrm{I}}\tau_{q_{\mathrm{II}}} + \frac{K_{\mathrm{I}}\tau_{q_{\mathrm{II}}}\tau_{T_{\mathrm{I}}}}{\Delta t} + K_{\mathrm{I}}\tau_{T_{\mathrm{I}}}\right)\frac{\partial T(L/2-\Delta x,t)}{\partial t}\right. \\ & + \left(K_{\mathrm{II}}\tau_{q_{\mathrm{I}}} + \frac{K_{\mathrm{II}}\tau_{q_{\mathrm{I}}}\tau_{T_{\mathrm{II}}}}{\Delta t} + K_{\mathrm{II}}\tau_{T_{\mathrm{II}}}\right)\left(\frac{\partial T(L/2+\Delta x,t)}{\partial t}\right) - (K_{\mathrm{I}}+K_{\mathrm{II}})\frac{\partial T(L/2,t)}{\partial t} + K_{\mathrm{I}}T(L/2-\Delta x,t) \\ & + K_{\mathrm{II}}T(L/2+\Delta x,t) + \left(\frac{K_{\mathrm{I}}\tau_{q_{\mathrm{II}}}\tau_{T_{\mathrm{I}}}}{\Delta t} + \frac{K_{\mathrm{II}}\tau_{q_{\mathrm{I}}}\tau_{T_{\mathrm{II}}}}{\Delta t}\right)\frac{\partial T(L/2,t-\Delta t)}{\partial t} \\ & \left. - \frac{K_{\mathrm{I}}\tau_{q_{\mathrm{II}}}\tau_{T_{\mathrm{I}}}}{\Delta t}\frac{\partial T(L/2-\Delta x,t-\Delta t)}{\partial t} - \frac{K_{\mathrm{II}}\tau_{q_{\mathrm{I}}}\tau_{T_{\mathrm{II}}}}{\Delta t}\frac{\partial T(L/2+\Delta x,t-\Delta t)}{\partial t}\right]. \end{aligned} \tag{32}$$

The interface temperature at new time step is calculated by Eq. (14) as

$$T(L/2,t+\Delta t) = T(L/2,t) + \Delta t\frac{\partial T(L/2,t)}{\partial t} + \frac{\Delta t}{2}\left[\frac{\partial T(L/2,t)}{\partial t} - \frac{\partial T(L/2,t-\Delta t)}{\partial t}\right]. \tag{33}$$

The interface temperature and boundary conditions at $x = 0$ and $x = L$ provide sufficient boundary conditions to calculate temperature distribution in Layers I and II.

3.4. Solution procedures

Numerical solutions are executed as the following procedures:

1. At time t, the directional particle distribution functions, $f_i(\mathbf{x},t)$, for each lattice are given.
2. The rate of temperature change and temperature are calculated respectively by Eqs. (13) and (14).
3. The equilibrium particle distribution function $f_i^{(0)}(\mathbf{x},t)$ are calculated according to Eq. (31).
4. The interfacial boundary condition for new time step is calculated.
5. The collision steps are executed to obtained the post-collision populations as

$$f_i(\mathbf{x},t+\Delta t) = f_i(\mathbf{x},t) - \frac{\Delta t}{\tau}\left[f_i(\mathbf{x},t) - f_i^{(0)}(\mathbf{x},t)\right] - 2A\Delta t\frac{\partial T(\mathbf{x},t)}{\partial t} + \Delta t\Psi.$$

6. The lattice populations are then shifted in the streaming step by

$$f_i(\mathbf{x}+\mathbf{e}_i\Delta t, t+\Delta t) = f_i(\mathbf{x},t+\Delta t).$$

3.5. Verification of numerical scheme and computer code

Before presenting the transmission–reflection phenomena in the two-layered structure within the DPL framework, the validity of the proposed numerical method is tested. In the first tested example, the temperature distribution in a semi-infinite slab at a particular time for three different values of phase lag ratio, B, is examined. The dimensionless boundary temperature at $x = 0$ of the slab was raised from 0 to 1 at $t = 0^+$. This example has been solved analytically by Tzou [4]. As shown in Fig. 3, the agreement between the analytical solutions and the present numerical results is very good.

In the second tested example, a pulsed volumetric heat source of width l emanating from Layer I adjacent to the exterior surface at $x = 0$ is considered. This dimensionless heat source is mathematically represented as

$$G(x,t) = \begin{cases} \dfrac{\delta(t)}{l}, & 0 \leqslant x \leqslant l \\ 0, & x > l \end{cases}. \tag{34}$$

This example was studied by Frankel et al. [1] within the framework of HHCE, which be retrieved from the current numerical scheme simply by letting $\tau_{T_{\mathrm{I}}} = \tau_{T_{\mathrm{II}}} = 0$. At $t = 0^+$, a dimensionless heat source of strength of 20 was imposed within $x = 0$ to l, $l = 0.05$. Effects of thermal conductivity, diffusivity, and relaxation time τ_q on the reflection–trans-

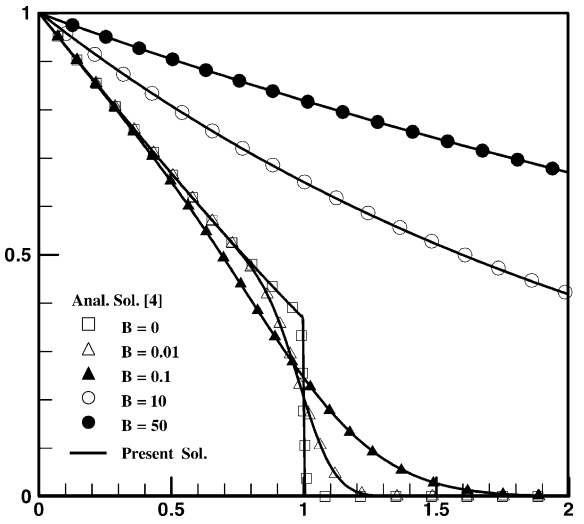

Fig. 3. Diagram showing comparison of the temperature distribution between analytical solution and the present numerical solution for three values of lag ratio, B.

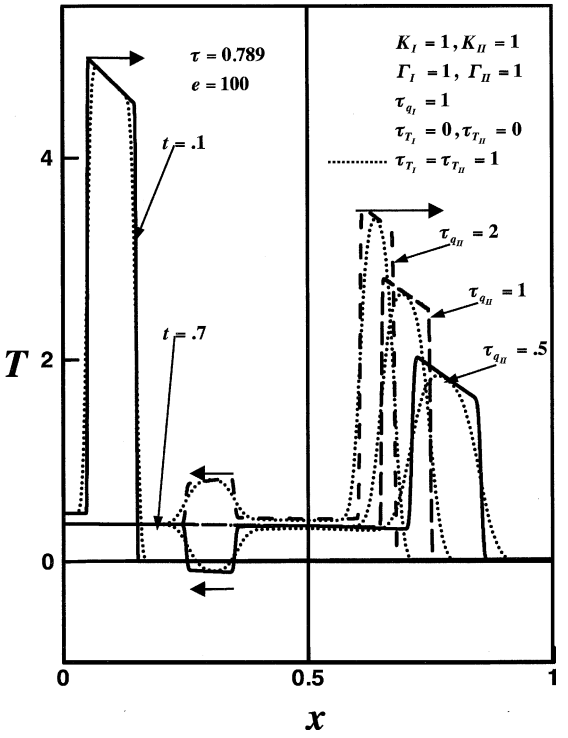

Fig. 4. Retrieving computational results presented in the literature [1] by the current numerical scheme for verification of numerical scheme. Effect of $\tau_{q\text{II}}$ on temperature distribution at two particular times $t = 0.1$ and 0.7 are shown. The dot line ones indicate the influence of τ_T was taken into consideration.

mission phenomena described in the literature [1] were tested. All the wave behaviors described in the literature were able to be retrieved from the present numerical scheme. Fig. 4 presents one of the test result.

4. Results and discussion

Effects of the material properties K, Γ, and τ_q on the reflection–transmission phenomena at interface have been discussed comprehensively by Frankel et al. [1] in the framework of HHCE. This study, therefore, mainly focuses on the effect of τ_T on the fundamental nature of heat transfer at layer interface within the DPL framework. Mathematically, the energy absorption within the penetration layer is described by Eq. (34).

In Fig. 4, results presented by the dot lines were calculated using the same material properties as their corresponding lines but with a finite value of τ_T that was set as $\tau_{T_{\rm I}} = \tau_{T_{\rm II}} = 1$. It was demonstrated by Eq. (11) that the interfacial boundary condition based on the DPL model is reduced to that for the HHCE when $\tau_{T_{\rm I}} = \tau_{T_{\rm II}}$. Thus, no extra reflection–transmission phenomena are induced when the pulsed thermal energy passing through the interface. From Eq. (5) the contribution of τ_T is from the term of the mixed spatial and time derivative, $\Gamma B\partial^3 T/(\partial t\,\partial x^2)$. This term can be interpreted as diffusing the dissipation effect out with the effective coefficient of "diffusivity" ΓB that results in blunting the sharp waveforms and broadening wave range. It is noted, from this figure, that a reflected negative temperature is also possible within the DPL framework.

To discuss the effect of τ_T on the reflection–transmission phenomena resulting from the interface, all material properties for the two layers were chosen to be the same except the τ_T, i.e. $\tau_{T_{\rm I}} \neq \tau_{T_{\rm II}}$. Fig. 5 shows the distribution of temperature at two particular times $t = 0.1$ and 0.7 for both $\tau_{T_{\rm II}} = 0.001$ (dash line) and $\tau_{T_{\rm II}} = 0.02$ (solid line) as $\tau_{T_{\rm I}}$ was kept at 0.001. At $t = 0.1$, both the solid and dash lines were coincided with each other, because the temperature wave was still in Layer I and the effect of $\tau_{T_{\rm II}}$ from Layer II didn't play a significant role in upstream temperature distribution yet. Since V was chosen to be unitary, the "apparent" thermal wave arrived the interface around $t = 0.45$. After this time, the effect of thermal wave on Layer II was observed. For $\tau_{T_{\rm II}} = \tau_{T_{\rm I}} = 0.001$, the thermal wave transmits the interface without any reflection. Compared with the waveform at $t = 0.1$, the magnitude of the transmitted wave at $t = 0.7$ was reduced and waveform is further blunted and spread due to the dissipation mechanism. For $\tau_{T_{\rm II}} = 0.02$,

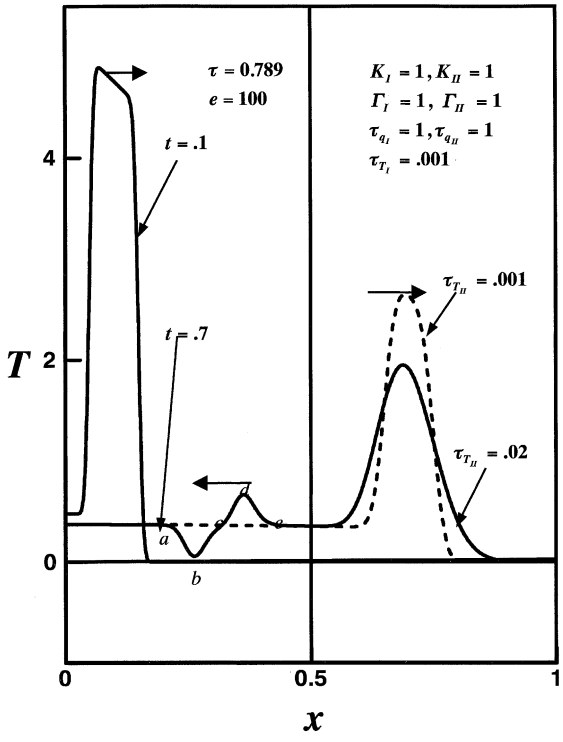

Fig. 5. Temperature distributions for $\tau_{T_{\rm II}} = 0.001$ and 0.02 at $t = 0.1$ and 0.7. All other material properties for the two layers were assumed to be unitary and $\tau_{T_{\rm I}}$ was set to be 0.001.

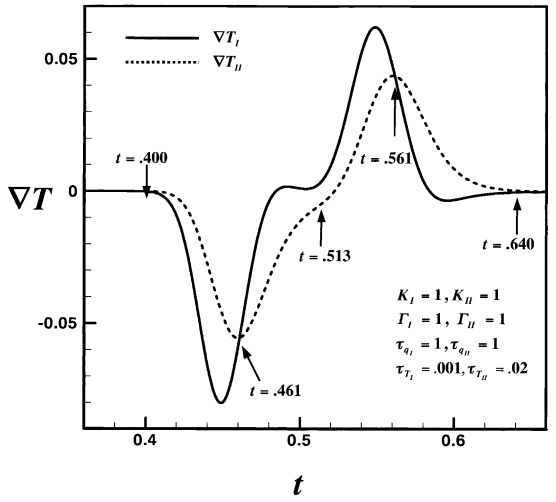

Fig. 6. Diagram showing temperature gradients, ∇T_{I} and ∇T_{II}, as a function of time.

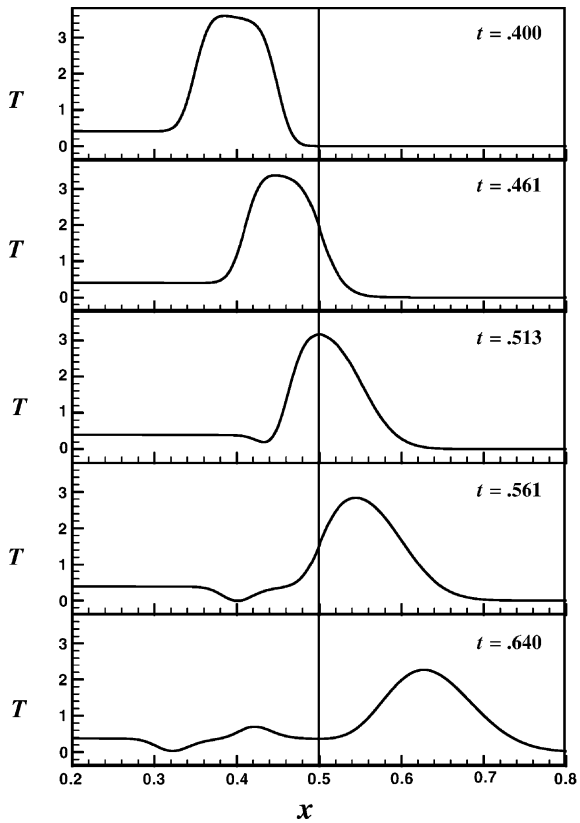

Fig. 7. Temperature distributions at five times $t = 0.40$, 0.46, 0.51, 0.56, and, 0.64. These times were within the period the pulsed thermal wave reached, passed, and left the interface. Material properties are described in Fig. 6.

when the wavefront reached the interface, it was split into two waves traveling in opposing directions. The transmitted wave, traveling to the right, retained the initial wavelike features. Compared with the waveform of the transmitted wave for $\tau_{T_{\rm I}} = 0.001$, the waveform for $\tau_{T_{\rm II}} = 0.02$ is smaller in magnitude and more spread in space. The reflected wave, traveling to the left, showed unusual features, however. The layer interface first reflected back a relatively negative wavefront then followed by a positive one, as labeled by lowercase letters *a*,*b*,*c*,*d*, and *e* at $t = 0.7$.

To discuss these special features resulted from the DPL heat conduction equation, the interfacial boundary condition is examined. With the chosen material properties of $K_{\rm I} = K_{\rm II} = K$ and $\tau_{q_{\rm I}} = \tau_{q_{\rm II}}$, Eq. (10) is reduced to

$$-K\frac{\partial T_{\rm I}}{\partial x} - K\tau_{T_{\rm I}}\frac{\partial^2 T_{\rm I}}{\partial x\,\partial t} = -K\frac{\partial T_{\rm II}}{\partial x} - K\tau_{T_{\rm II}}\frac{\partial^2 T_{\rm II}}{\partial x\,\partial t}. \tag{35}$$

Expanding temperature gradients on both sides with respect to $\tau_{T_{\rm I}}$ and$\tau_{T_{\rm II}}$, Eq. (35) can be approximated

$$-K\nabla T_{\rm I}(t+\tau_{T_{\rm I}}) \approx -K\nabla T_{\rm II}(t+\tau_{T_{\rm II}}), \tag{36}$$

when $\tau_{T_{\rm I}}$ and $\tau_{T_{\rm II}}$ are small. This expression indicates that there is a time shift of $\tau_{T_{\rm II}} - \tau_{T_{\rm I}}$ between $\nabla T_{\rm I}$ and $\nabla T_{\rm II}$. Fig. 6 shows temperature gradients on both sides of the interface, $\nabla T_{\rm I}$ and $\nabla T_{\rm II}$, as a function of time. The time lag between these two temperature-gradient waves is clearly shown. In addition to the phase shift, the wave amplitude for $\nabla T_{\rm II}$ is smaller due to the higher τ_T in Layer II. Roughly four stages can be specified according to five particular times at $t = 0.40$, 0.46, 0.51, 0.56 and 0.64. Temperature distributions in the computational region for these five times are shown in Fig. 7. These times were within the period that the thermal wave reached, passed through, and left the interface.

In the study of the transmission–reflection phenomena of wave resulting from layer interface within the HHCE framework [1], when the pulsed thermal wave reached the interface a relatively negative temperature wavefront was reflected if Layer II had a less resistance, $K_{\rm II} > K_{\rm I}$, that caused more energy to enter Layer II. On the opposite, a

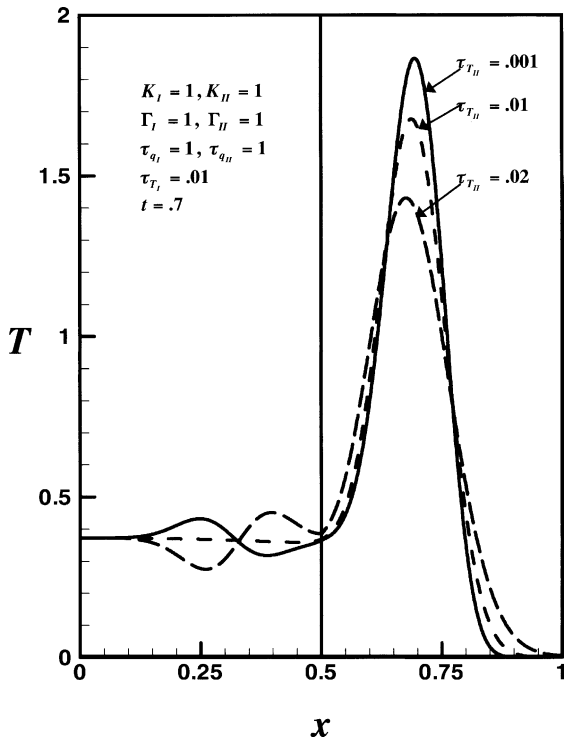

Fig. 8. Effect of $\tau_{T_{\rm II}}$ on the transmission–reflection phenomena at $t = 0.7$. $\tau_{T_{\rm I}} = 0.01$. Temperature distribution for three values of $\tau_{T_{\rm II}}$, $\tau_{T_{\rm II}} = 0.001$ ($< \tau_{T_{\rm I}}$), $\tau_{T_{\rm II}} = 0.01$ ($= \tau_{T_{\rm I}}$), and $\tau_{T_{\rm II}} = 0.02$ ($> \tau_{T_{\rm I}}$), are shown.

relatively positive temperature wavefront was reflected if $K_I > K_{II}$. By analogy with this argument, Eq. (36) can be numerically expressed in terms of an effective thermal conductivity and temperature gradients for a particular time t as

$$-K'_I \nabla T_I(t) = -K'_{II} \nabla T_{II}(t), \tag{37}$$

where K' is the effective thermal conductivity. During the first stage, $t = 0.40$–0.46, since $\nabla T_I < \nabla T_{II} < 0$, or $K'_{II} > K'_I$, a relatively temperature decreasing wavefront was reflected back to Layer I from the interface due to the less resistance in Layer II. This stage was in charge to the generation of the portion from a to b of the reflected wave in Fig. 5. For the second stage, $t = 0.46$–0.51, $\nabla T_{II} < \nabla T_I < 0$, or $K'_{II} < K'_I$, an temperature increasing wavefront was reflected from the interface because of the higher effective thermal resistance of Layer II. This stage corresponded to portion from b to c of the reflected wave in Fig. 5. For these first two stages, the interface temperature was increased and caused negative ∇T_{II} and ∇T_I because they were in the duration the rising part of the thermal wave crossing the interface, see Fig. 7. The last two stages, $t = 0.51$–0.56 and 0.56–0.64, corresponded to the declining portion of the thermal wave that resulted in positive ∇T_{II} and ∇T_I. Being opposite to the first two stages, the last two stages first reflected an increasing followed by an decreasing temperature wavefront from the interface, which were matching the portions c to d and d to e in Fig. 5.

In Fig. 8, the temperature distribution at $t = 0.7$ was shown for three values of $\tau_{T_{II}}$, 0.001, 0.01, and 0.02 while τ_{T_I} was kept at 0.01. When $\tau_{T_{II}} < \tau_{T_I}$, the interface first reflected back a relatively positive then followed by a negative wavefront. Thus, the reflected wave for $\tau_{T_{II}} < \tau_{T_I}$ was out of phase to that for $\tau_{T_{II}} > \tau_{T_I}$. With the increasing of $\tau_{T_{II}}$, the dissipation effect resulting from the mixed derivative term, $\Gamma B \partial^3 T/(\partial x^2 \partial t)$, in Layer II was more effective that diminished the wave amplitude with broadening the wave range in space.

5. Conclusions

In this study, the heat transfer and the transmission–reflection phenomenon, induced by a pulsed thermal energy passing through the layer interface of a two-layered structure, are studied numerically. Both the governing equation and the interfacial conditions, based on the continuities of temperature and heat flux, within the framework of DPL model are derived and discussed. An extended, discretized LB equation and a numerical solution procedure are developed to solve the equations. The technique of Chapman–Enskog multiscale expansion shows that the proposed extended LB equation macroscopically matches the governing equation with truncation error of order two. The test examples show that the results obtained by the present numerical scheme agree very well with analytical or numerical solutions in the literature.

The fundamental difference between the hyperbolic and DPL based heat conduction equations is the extra phase lag time, τ_T. This time lag introduces an additional mechanism of diffusion the dissipation effect in the governing equation as well as new mixed spatial and time derivatives for interfacial boundary condition. These mixed derivatives lead to fundamental different transmission–reflection phenomena from the layer interface. With the passing of a pulsed thermal wave, the interface either reflects a negative or a positive wavefront in the framework of HHCE. For the DPL based system, the interface can reflect a negative wavefront followed by a positive one when $\tau_{T_{II}} > \tau_{T_I}$ and vice versa if $\tau_{T_{II}} < \tau_{T_I}$. This special features can be attributed to the time shift between ∇T_I and ∇T_{II} that results in sinusoidal difference between the effective thermal conductivities on two sides of the interface.

Acknowledgements

Support for this work by the National Science Counsel of the Republic of China under Grant no. NSC90-2212-E-194-026 is gratefully acknowledged.

References

[1] J.I. Frankel, B. Vick, M.N. Ozisik, General formulation and analysis of hyperbolic heat conduction in composite media, Int. J. Heat Mass Transfer 30 (7) (1987) 1293–1305.
[2] C. Cattaneo, A form of heat conduction equation which eliminates the paradox of instantaneous propagation, Compte Rendus 247 (1958) 431–433.
[3] P. Vernotte, Some possible complications in the phenomena of thermal conduction, Compte Rendus 252 (1961) 2190–2191.
[4] D.Y. Tzou, in: Macro-to microscale heat transfer: the lagging behavior, Taylor & Francis, Washington, DC, 1996, pp. 25–29.
[5] D.D. Joseph, L. Preziosi, Heat waves, Rev. Mod. Phys. 61 (1) (1989) 41–73.

[6] D.D. Joseph, L. Preziosi, Addendum to the paper "Heat waves", Rev. Mod. Phys. 62 (2) (1990) 375–391.
[7] M.N. Ozisik, D.Y. Tzou, On the wave theory in heat conduction, J. Heat Transfer, ASME Trans. 116 (1994) 526–535.
[8] Y. Taitel, On the parabolic, hyperbolic and discrete formulation of the heat conduction equation, Int. J. Heat Mass Transfer 15 (1972) 369–371.
[9] C. Korner, H.W. Bergmann, The physical defects of the hyperbolic heat conduction equation, Appl. Phys. A 67 (1998) 397–401.
[10] C. Bai, A.S. Lavine, On the hyperbolic heat conduction and the second law of thermodynamics, J. Heat Transfer, ASME Trans. 117 (1995) 256–263.
[11] D.Y. Tzou, A unified field approach for heat conduction from micro-to macro-scales, J. Heat Transfer, ASME Trans. 117 (1995) 8–16.
[12] D.Y. Tzou, The generalized lagging response in small-scale and high-rate heating, Int. J. Heat Mass Trans. 38 (1995) 3231–3240.
[13] D.Y. Tzou, Experimental support for the lagging response in heat propagation, AIAA J. Thermophys. Heat Transfer 9 (1995) 686–693.
[14] M.A. Al-Nimr, N.S. Al-Huniti, Transient thermal stresses in a thin elastic plate due to a rapid dual-phase-lag heating, J. Thermal Stresses 23 (2000) 731–746.
[15] D.Y. Tzou, J.K. Chen, Thermal lagging in random media, J. Thermophys. Heat Transfer 12 (4) (1998) 567–574.
[16] P.J. Antaki, Solution for non-Fourier dual phase lag heat conduction in a semi-infinite slab with surface heat flux, Int. J. Heat Mass Transfer 41 (14) (1998) 2253–2258.
[17] M.A. Al-Nimr, M. Naji, V.S. Arbaci, Nonequilibrium entropy production under the effect of the dual-phase-lag heat conduction model, ASME J. Heat Transfer 122 (2000) 217–222.
[18] M. Al-Nimr, M. Naji, On the phase-lag effect on the nonequilibrium entropy production, Microscale Thermophys. Eng. 4 (2000) 231–243.
[19] D.Y. Tzou, K.K.S. Chiu, Depth of thermal penetration: effect of relaxation and thermalization, J. Thermophys. Heat Transfer 13 (2) (1999) 266–269.
[20] P.J. Antaki, Effect of dual-phase-lag heat conduction on ignition of a solid, J. Thermophys. Heat Transfer 14 (2) (2000) 276–278.
[21] D.Y. Tzou, K.S. Chiu, Temperature-dependent thermal lagging in ultrafast laser heating, Int. J. Heat Mass Transfer 44 (2001) 1725–1734.
[22] J.K. Chen, J.E. Beraun, D.Y. Tzou, A dual-phase-lag diffusion model for predicting thin film growth, Semicond. Sci. Technol. 15 (2000) 235–241.
[23] J.K. Chen, J.E. Beraun, D.Y. Tzou, A dual-phae-lag diffusion model for interfacial layer growth in metal matrix composites, J. Mater. Sci. 34 (1999) 6183–6187.
[24] J.K. Chen, J.E. Beraun, D.Y. Tzou, A dual-phase-lag diffusion model for predicting intermetallic compound layer growth in solder joints, ASME J. Electron. Packaging 123 (2001) 52–57.
[25] D.G. Cahill, Heat transport in dielectric thin films and at solid–solid interfaces, in: C.L. Tien, A. Majumdar, F.M. Gerner (Eds.), Microscale energy transport, Taylor & Francis, Washington, DC, 1998, pp. 95–117.
[26] M.N. Ozisik, B. Vick, Propagation and reflection of thermal waves in a finite medium, Int. J. Heat Mass Transfer 37 (10) (1984) 1845–1854.
[27] D.Y. Tzou, Reflection and refraction of thermal waves from a surface or an interface between dissimilar materials, Int. J. Heat Mass Transfer 36 (2) (1993) 401–410.
[28] W.-B. Lor, H.-S. Chu, Propagation of thermal waves in a composite medium with interface thermal boundary resistance, Numer. Heat Transfer A 36 (1999) 681–697.
[29] W.-B. Lor, H.-S. Chu, Effect of interface thermal resistance on heat transfer in a composite medium using the thermal wave model, Int. J. Heat Mass Transfer 43 (2000) 653–663.
[30] T.Q. Qiu, C.L. Tien, Femtosecond laser heating of multi-layer metals-I. Analysis, Int. J. Heat Mass Transfer 37 (17) (1994) 2789–2797.
[31] J.R. Ho, C.P. Grigoropolous, J.A.C. Humphrey, Computational study of heat transfer and gas dynamics in the pulsed laser evaporation of metals, J. Appl. Phys. 78 (7) (1995) 4696–4709.
[32] N. Angelucci, N. Bianco, Thermal transient analysis of thin film multilayers heated by pulsed laser, Int. J. Heat Mass Transfer 40 (18) (1997) 4487–4491.
[33] A.K. Gunstensen, D.H. Rothman, S. Zaleski, G. Zanetti, Lattice Boltzmann model of immiscible fluids, Phys. Rev. A 43 (1991) 4320–4327.
[34] X. Shan, H. Chen, Lattice Boltzmann model for simulating flows with multiple phases and components, Phys. Rev. E 47 (1993) 1815–1819.
[35] F.J. Alexander, S. Chen, J.D. Sterling, Lattice Boltzmann thermodynamics, Phys. Rev. E 47 (1993) 2249–2252.
[36] X. Shan, Simulation of Rayleigh-Benard convection using a lattice Boltzmann method, Phys. Rev. E 55 (1997) 2780–2788.
[37] S. Chen, G.D. Doolen, Lattice Boltzmann method for fluid flows, Annu. Rev. Fluid Mech. 30 (1998) 329–364.
[38] D. Wolf-Gladrow, Lattice-gas cellular automata and lattice Boltzmann models: An introduction, Springer-Verlag, Berlin, Heidelberg, 2000.
[39] D. Wolf-Gladrow, A lattice Boltzmann equation for diffusion, J. Stat. Phys. 79 (1995) 1023–1032.
[40] W.S. Jiaung, J.R. Ho, C.P. Kuo, Lattice Boltzmann method for heat conduction problem with phase change, Numer. Heat Transfer B 39 (2001) 167–187.

[41] G. Yan, A lattice Boltzmann equation for waves, J. Comput. Phys. 161 (2000) 61–69.
[42] R.G.M. van der Sman, M.H. Ernst, A.C. Berkenbosch, Lattice Boltzmann scheme for cooling of packed cut flows, Int. J. Heat Mass Transfer 43 (2000) 577–587.
[43] G.S. Prakash, S.S. Reddy, S.K. Das, T. Sundararajan, K.N. Seetaramu, Numerical modelling of microscale effects in conduction for different thermal boundary conditions, Numer. Heat Transfer A 38 (2000) 513–532.